XVI International Conference on Computational Plasticity. Fundamentals and Applications
COMPLAS 2021
E. Oñate, D. Peric, M. Chiumenti and Eduardo de Souza Neto (Eds)

# EFFECTS OF THE STRESS INVARIANTS $I_1$ AND $J_3$ ON THE FATIGUE BEHAVIOR OF METALLIC MATERIALS

**ARAÚJO L.M * AND MALCHER L.***

* University of Braília (UnB)
Mechanical Engineering Department
Campus nDarcy Ribeiro, Asa Norte, Braslia, Brazil
e-mail: lucasmangas96@gmail.com

**Key words:** Stress Invariants, Low Cycle Fatigue and Ultra-Low Cycle Fatigue

**Abstract.**

**Abstract.** The objective of the present work is to evaluate the effects of the stress invariants $I_1$ and $J_3$ on the fatigue behavior of metallic materials. In this regard, the Ultra-Low (ULCF) and Low (LCF) Cycle fatigue behavior of SAE 1045 steel was analyzed supported by the data from by Bai [1] and Leese and Socie [2]. Furthermore, a Gao-based model [3] with mixed hardening was proposed to capture the influence $I_1$ and $J_3$ mechanical response. The numerical simulations conducted using a von Mises approach did not properly agreed with the experimental data, which demonstrated the SAE 1045 dependence on $I_1$ and $J_3$. After the calibration of Gao's parameters $a$ and $b$, the numeric results displayed better agreement with respect to the numerical data. The most pronounced between traditional $J_2$ and invariants sensitive modeling arose in the Ultra-Low cycle conditions, while the discrepancies in the LCF regime were less substantial. Nevertheless, the evolution of the accumulated plastic strain expected by Mises ang Gao approaches in LCF situations deviated considerably, which suggests that the proposed formulation may be an attractive option for fatigue life assessments via incremental techniques.

## 1 INTRODUCTION

Fatigue is a type of failure experienced by structures and components subjected to dynamical loads, and hence is a major concern in engineering design. One of the key information sought by engineers is the component expected fatigue life $N_f$, which can be estimated by many techniques [4, 5, 6]. Regardless of the approach used, the accuracy of the prediction strongly depends on the choice of a constitutive model for the simulation of the material cyclic behavior, specially in Ultra-Low and Low Cycle fatigue regimes (ULCF and LCF, respectively). von Mises or $J_2$ constitutive models are traditionally chosen due to its simplicity and satisfactory results in some applications. However, some metallic materials exhibit an elastoplastic behavior between Tresca and Mises yield surfaces, which is an observation well acknowledged in Ductile Fracture applications [7, 8, 9]. This latter indicates that the theses alloys are $I_1$ and $J_3$ sensitive. If the material monotonic behavior is affected by the stress invariants, one can expect that its cyclic response will likely be influenced by these parameters.

In this setting, this contribution aims to investigate the consequences of using a $I_1$ and $J_3$ sensitive model for the description of the cyclic behavior of SAE 1045 steel alloy. Therefore, a Gao-based model [3] with mixed hardening is proposed and numerically implemented to simulate the ULCF and LCF response of SAE 1045 steel. Mises and Gao simulations were conducted and compared with the data available in [1, 2].

## 2 THEORETICAL FRAMEWORK

### 2.1 Cauchy Stress Decomposition and Invariants Definition

The stress state in a given material point can be characterized by the Cauchy stress tensor $\boldsymbol{\sigma}$ at that point. $\boldsymbol{\sigma}$ may be uniquely decomposed into a deviatoric $\boldsymbol{S}$ and volumetric $p\boldsymbol{I}$ parts

$$\boldsymbol{\sigma} = \boldsymbol{S} + p\boldsymbol{I}. \tag{1}$$

The principal invariants $I_i$, $i = 1, 2, 3$ of $\boldsymbol{\sigma}$ provide a frame-independent characterization of the stress state. These invariants are defined as:

$$\begin{cases} I_1(\boldsymbol{\sigma}) = \operatorname{tr}(\boldsymbol{\sigma}), \\ I_2(\boldsymbol{\sigma}) = \dfrac{1}{2}\left[\operatorname{tr}^2(\boldsymbol{\sigma}) - \operatorname{tr}(\boldsymbol{\sigma}^2)\right], \\ I_3(\boldsymbol{\sigma}) = \det(\boldsymbol{\sigma}), \end{cases} \tag{2}$$

where $\operatorname{tr}(\cdot)$ and $\det(\cdot)$ express the trace and determinant operations respectively. It is worth noting that Eq.2 implies that the hydrostatic stress is one third of $I_1$. The invariants $J_i$ of $\boldsymbol{S}$ are relevant in plasticity theory, and are computed by:

$$\begin{cases} J_2(\boldsymbol{S}) = \dfrac{1}{2}\boldsymbol{S} : \boldsymbol{S} \\ J_3(\boldsymbol{S}) = \det(\boldsymbol{S}), \end{cases} \tag{3}$$

in which : represents the double contraction product, commonly referred to as the inner product between second order tensors.

### 2.2 Key Features of the Gao-based Elatoplastic Model

The yield criterion $\phi$ proposed is:

$$\phi = \sigma_{eq}(\boldsymbol{\eta}) - \sigma_y(\bar{\varepsilon}^p) \leq 0. \tag{4}$$

in which $\boldsymbol{\eta}$, $\sigma_y$ and $\bar{\varepsilon}^p$ respectively denote the relative stress tensor, yield strength and accumulated plastic strain. Due to the model presure dependence, $\boldsymbol{\eta}$ is defined as:

$$\boldsymbol{\eta}(\boldsymbol{\sigma}, \boldsymbol{\beta}) : = \boldsymbol{\sigma} - \boldsymbol{\beta}, \tag{5}$$

with $\boldsymbol{\beta}$ representing the backstress tensor. The increase of $\sigma_y$ due to plastic flow is described by Kleinermann and Ponthot[10] 4 parameters hardening law :

$$\sigma = \sigma_{y0} + \omega\bar{\varepsilon}^p + (\sigma_\infty - \sigma_{y0})\left[1 - \exp\left(-\delta\bar{\varepsilon}^p\right)\right], \tag{6}$$

where $\sigma_{y0}$ is the initial yield stress. Gao's equivalent stress $\sigma_{eq}(\boldsymbol{\eta})$ is defined as:

$$\sigma_{eq} = c\left(aI_1^6 + 27J_2^3 + bJ_3^2\right)^{\frac{1}{6}}, \tag{7}$$

with $a, b$ and $c$ denoting material parameters. $c$ is constrained by $a$ and $b$ by the relation:

$$c = \left(a + \frac{4}{729}b + 1\right)^{\frac{-1}{6}}. \tag{8}$$

The flow law dicating the evolution $\dot{\boldsymbol{\varepsilon}}^p$ of the plastic strain tensor $\boldsymbol{\varepsilon}^p$ is based on the associativity assumption:

$$\dot{\boldsymbol{\varepsilon}}^p = \dot{\gamma}\frac{\partial\phi}{\partial\boldsymbol{\sigma}} = \dot{\gamma}\boldsymbol{N}, \tag{9}$$

in which $\boldsymbol{N}$ represents the flow vector. The evolution $\dot{\bar{\varepsilon}}^p$ of the accumulated plastic strain is defined by:

$$\dot{\bar{\varepsilon}}^p = \dot{\gamma}\frac{\boldsymbol{\eta}\colon\boldsymbol{N}}{\sigma_y\left(\bar{\varepsilon}^P\right)}, \tag{10}$$

where $\dot{\gamma}$ is the plastic multiplier. Finally, the Armstrong-Frederick kinematic hardening law was chosen for the evolution $\dot{\boldsymbol{\beta}}$ of the backstress tensor:

$$\dot{\boldsymbol{\beta}} = \frac{2}{3}H^K\dot{\boldsymbol{\varepsilon}}^p - \dot{\bar{\varepsilon}}^p b^K\boldsymbol{\beta}, \tag{11}$$

with $H^K$ and $b^K$ denoting the kinematic hardening modulus and saturation coefficient, respectively.

## 3 NUMERICAL METHODOLOGY

The constitutive model briefly described in section 2 was numerically solved basedon operator decomposition technique [11]. The numerical integration of the plastic corrector phase was conducted by an implicit scheme. The referred technique was incorporated in the academic Finite Element code HYPLAS [11] and it was coded in MATLAB for Gauss point level simulations.

## 4 DATA AND CALIBRATION

The Ultra-Low Cycle regime can be viewed as the frontier between Ductile Fracture and Low Cycle fatigue, and hence ULCF will display features from both regimes. Indeed, authors usually assume mixed hardening conditions in ULCF, which means that both isotropic and kinematic hardening take place. One needs a standard tensile test to

calibrate the hardening parameters in Eq.6, while a set of cyclic tests in the Utra-Low cycle regime is required for the identifaction of the kinematic constants in Eq.11. These are available in [1], and after the calibration process, one arrives at the values given in Table 1.

**Table 1**: Material parameters calibrated for the SAE 1045 ULCF conditions based on the data from [1]. These constants were used in the ULCF simulations.

| Parameter | Value |
|---|---|
| Elasticity Modulus $E$ | 178.9 GPa |
| Poisson's Ratio $\nu$ | 0.3 |
| Monotonic Yield Stress $\sigma_{y0}$ | 725.0 MPa |
| $\omega$ | 347.6 MPa |
| $\sigma_\infty$ | 890.4 MPa |
| $\delta$ | 405.5 |
| Kinematic Hardening Modulus $H^K$ | 2319.1 MPa |
| Saturation Coefficient $b^K$ | 16.4 |

The LCF simulations considered only kinematic hardening, and the required materials parameters calibrated with the fully reversed tension tests in [2]. The outcome of the identification process are presented in Table 2.

**Table 2**: Material parameters calibrated for the SAE 1045 in LCF conditions based on the data from [2]. These constants were used in the LCF simulations.

| Parameter | Value |
|---|---|
| Elasticity Modulus $E$ | 202.0 GPa |
| Poisson's Ratio $\nu$ | 0.3 |
| Cyclic Yield Stress $\sigma_{y0}$ | 268.6 MPa |
| Kinematic Hardening Modulus $H^K$ | 32355.0 MPa |
| Saturation Coefficient $b^K$ | 122.5 |

Regarding the identification of Gao's $a$ and $b$ constants, one performed a trial an error method. First, Mises simulations in shear conditions with the parameters in Tables 1

and 2 were carried out and then compared with the ULCF and LCF data. Next, several simulations with different $b$ are conducted until a good agreement with respect to the experiments is reached. Finally, with the identified $b$, the same process is once more conducted, but this time with supported by the tensile tests to the estimation of $a$.

## 5 RESULTS

Figures 1 and 2 compares the reaction curves predicted by Mises-based formulation ($a = b = 0$) and by the proposed model for ULCF shear test on SAE 1045 steel butterfly specimen.

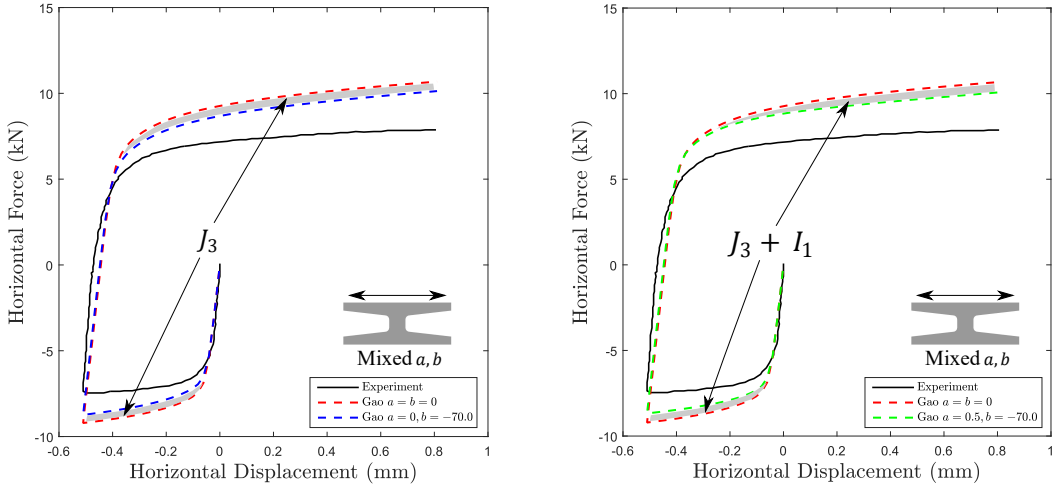


**Figure 1**: Comparison between the numerical responses of Mises and Gao based formulations with the experimental reaction curve from the shear-shear ($-0°$to$+0°$) test 1 after recalibration. On the left, only $b$ is activated, while on the left both $a$ and $b$ are considered.

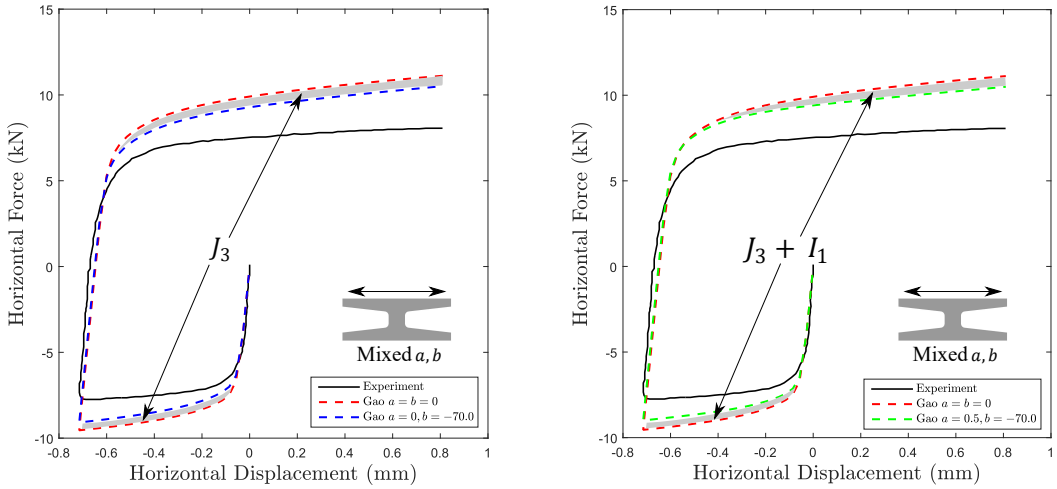


**Figure 2**: Comparison between the numerical responses of Mises and Gao based formulations with the experimental reaction curve from the shear-shear $(-0°\text{to}+0°)$ test 2 after recalibration. On the left, only $b$ is activated, while on the left both $a$ and $b$ are considered.

One observes that SAE 1045 steel is sensitive to $J_3$, which is demonstrated by the inaccuracy of the Mises predicted Force $F$ versus $d$ curve. The numerical curves obtained by the proposed formulation is closer to the experimental ones. Furthermore, the first invariant has a negligible effect on revered shear case, which indicates that $J_3$ is the most influential parameter in shear-predominant situations. This latter remark was observed in monotonic conditions [1, 9].

Figures 3 and 4 displays the outcome of the simulations of the compression-tension tests on SAE 1045 butterfly specimens.

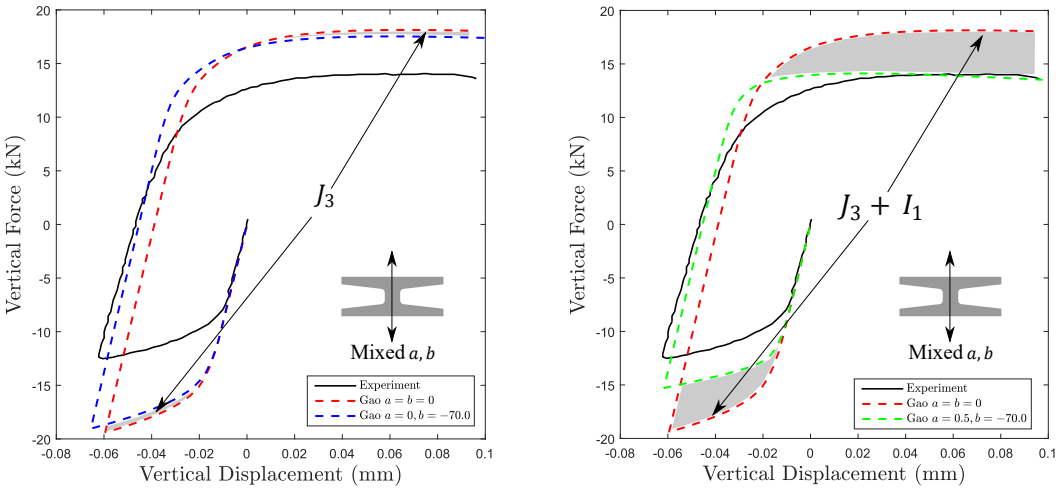


**Figure 3**: Comparison between the numerical responses of Mises and Gao based formulations with the experimental reaction curve from the compression-tension $(-90°\text{to}+90°)$ test 1 after recalibration. On the left, only $b$ is activated, while on the left both $a$ and $b$ are considered.

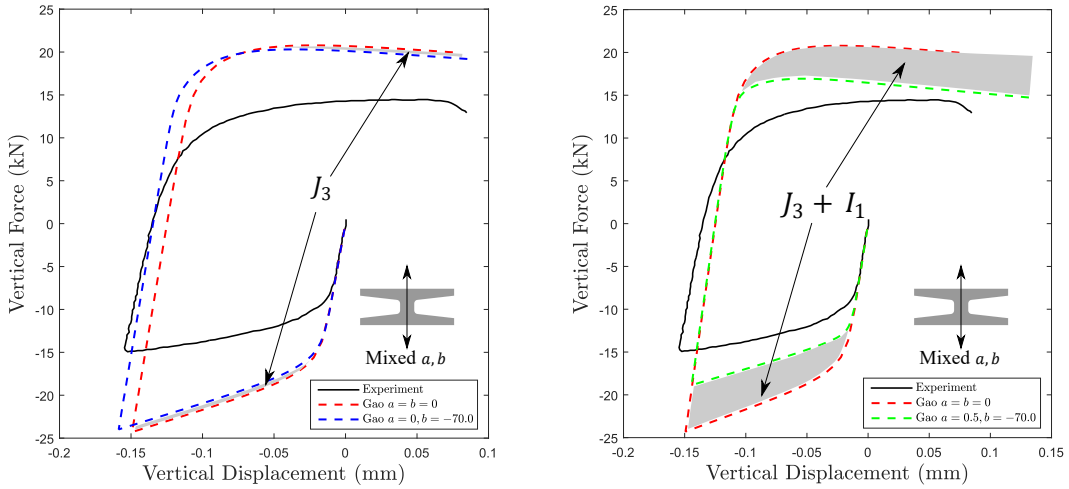


**Figure 4**: Comparison between the numerical responses of Mises and Gao based formulations with the experimental reaction curve from the compression-tension ($-90°$to$+90°$) test 2 after recalibration. On the left, only $b$ is activated, while on the left both $a$ and $b$ are considered.

Conversely from what was noted in Fig.1 and 2, the fist invariant is the key factor in the compression-tension behavior of SAE 1045 stell. Moreover, the numerical curves demonstrates that this alloy cyclic response depends on $I_1$ besides $J_3$.

Since Gao's and Mises's yield surfaces coincide in uniaxial stress states, the results from the fully reversed tension LCF simulations are not displayed in this work. Figure 5 shows the shear hysteresis loops predicted by Mises and Gao approaches in pure fully reversed torsion loading, while Fig.6 compares the shear stress amplitudes $\tau_a$ from each formulation with the mean experimental ones.

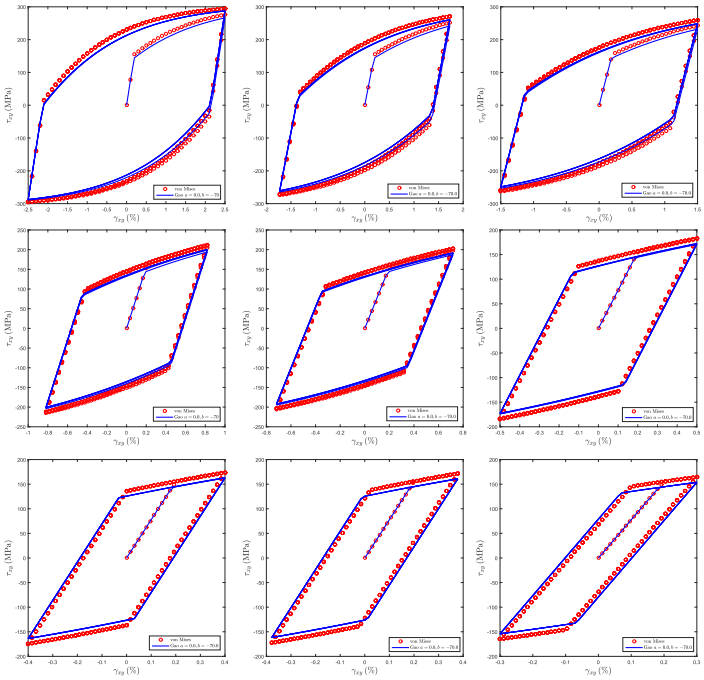

**Figure 5**: Shear hysteresis loops predicted by von Mises's (red circles) and Gao's (blue solid line) formulations for a range of shear strain amplitude $\gamma_a$.

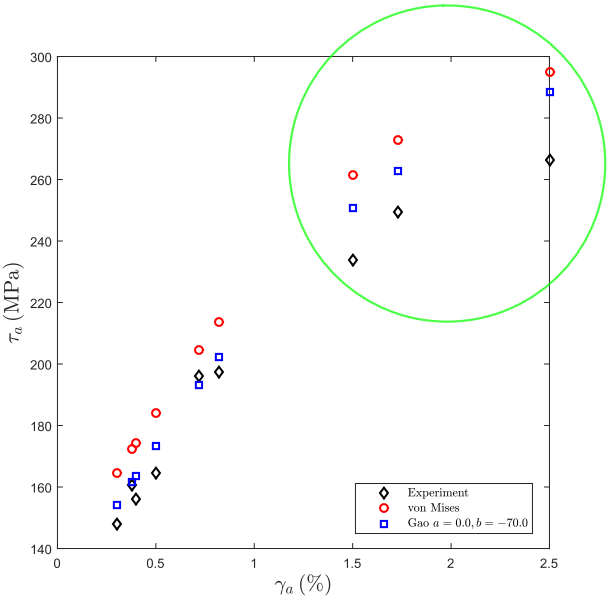


**Figure 6**: Comparison between normal stress amplitudes $\tau_a$ predicted by Mises's(red circles) and Gao's (blues squares), and the mean experimental amplitudes (black diamonds).

One notices from Fig.5 that there are differences between Mises and Gao loops,m although less substantial than observed in the ULCF tests. Furthermore, the proposed

constitutive modeling always furnished $\tau_a$ closer to the experimentally observed as depicted in Fig.6. The large discrepancies for high $\gamma_a$ highlighted in the green big circle are due to the limitations of Armstrong-Frederick evolution law. If Critical Plane fatigue life assessments are used, little gains are achieved in $N_f$ estimation are obtained due to its lack of sensibility to loop's size and shape [5]. Finally, Fig.7 presents the evolution of the accumulated plastic strain expected from the two formulations discussed for the highest and lowest shear strain amplitudes $\gamma_a$.

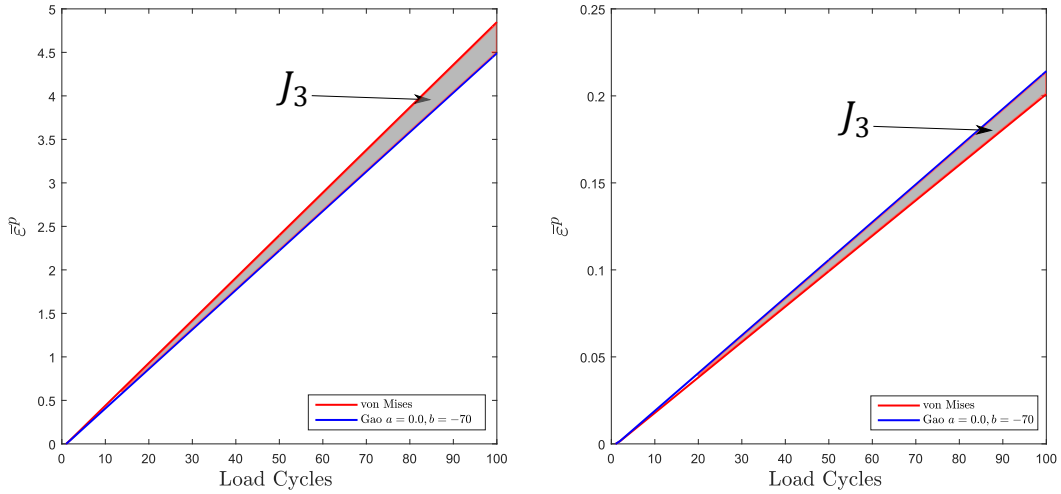


**Figure 7**: Predicted $\bar{\varepsilon}^p$ evolution by von Mises's and Gao's modeling. On the left the outcome for $\gamma$ =2.5% and on the right for $\gamma$ =0.3%.

It is observed from Fig.7 that Gao-based modeling foresees a slower evolution of $\bar{\varepsilon}^p$, which implies is higher fatigue lives in incremental approaches. Theses latter methods are more affected by the shape and size of the hysteresis loop, and hence considerable different $N_f$ assessments will be made depending on chosen constitutive modeling.

## 6 CONCLUSIONS

- SAE 1045 steel ULCF and LCF mechanical behaviors are $I_1$ and $J_3$ dependent. Nevertheless, the effects to these parameters on ULCF conditions were stronger than LCF;
- Better agreement with respective to experimental data were achieved by the proposed Gao-based model with mixed hardening;
- Fatigue life assessments in the Low Cycle regime may be improved by the usage of the constitutive formulation presented in this, especially if it is coupled with incremental approaches.

## REFERENCES

[1] Y. Bai, *Effect of Loading History on NecNing and Fracture, Massachusetts Institute of Technology*. PhD thesis, PhD thesis, 2008.

[2] G. E. Leese and D. Socie, *Multiaxial Fatigue: Analysis and Experiments: AE 14*. Society of Automotive Engineers, 1989.

[3] X. Gao, T. Zhang, J. Zhou, S. M. Graham, M. Hayden, and C. Roe, "On stress-state dependent plasticity modeling: Significance of the hydrostatic stress, the third invariant of stress deviator and the non-associated flow rule," *International Journal of Plasticity*, vol. 27, no. 2, pp. 217–231, 2011.

[4] A. Fatemi and D. F. Socie, "A critical plane approach to multiaxial fatigue damage including out-of-phase loading," *Fatigue & Fracture of Engineering Materials & Structures*, vol. 11, no. 3, pp. 149–165, 1988.

[5] Y. Jiang, W. Ott, C. Baum, M. Vormwald, and H. Nowack, "Fatigue life predictions by integrating evicd fatigue damage model and an advanced cyclic plasticity theory," *International Journal of Plasticity*, vol. 25, no. 5, pp. 780–801, 2009.

[6] L. Araújo, G. Ferreira, R. Neves, and L. Malcher, "Fatigue analysis for the aluminum alloy 7050-t7451 performed by a two scale continuum damage mechanics model," *Theoretical and Applied Fracture Mechanics*, vol. 105, p. 102439, 2020.

[7] L. Driemeier, M. Brünig, G. Micheli, and M. Alves, "Experiments on stress-triaxiality dependence of material behavior of aluminum alloys," *Mechanics of Materials*, vol. 42, no. 2, pp. 207–217, 2010.

[8] M. Brünig, S. Gerke, and V. Hagenbrock, "Micro-mechanical studies on the effect of the stress triaxiality and the lode parameter on ductile damage," *International Journal of Plasticity*, vol. 50, pp. 49–65, 2013.

[9] L. Malcher, L. Morales, V. Rodrigues, V. Silva, L. Araújo, G. Ferreira, and R. Neves, "Experimental program and numerical assessment for determination of stress triaxiality and j3 effects on aa6101-t4," *Theoretical and Applied Fracture Mechanics*, p. 102476, 2020.

[10] J.-P. Kleinermann and J.-P. Ponthot, "Parameter identification and shape/process optimization in metal forming simulation," *Journal of Materials Processing Technology*, vol. 139, no. 1-3, pp. 521–526, 2003.

[11] E. A. de Souza Neto, D. Peric, and D. R. Owen, *Computational methods for plasticity: theory and applications*. John Wiley & Sons, 2011.